International Journal of Grid Distribution Computing
Vol.7, no.3 (2014), pp.135-142
http://dx.doi.org/10.14257/ijgdc.2014.7.3.13

Comparative Study Between PI and Resonant Controllers for PV Grid-Connected Inverter

S. Makhloufi

LESSI Laboratory, University of ADRAR, ALGERIA
makhlofi_s@yahoo.fr

Abstract

Control of PV-grid connected inverter introduces a delay between sinusoidal current reference and measured current at the output of the inverter. This leads to a phase difference between the current injected by the inverter and grid voltage when using a simple PI controller. To overcome this problem, PI controllers used to control injected currents to the grid have been substituted, in this study, by resonant controllers. The obtained results show that phase difference between grid current and voltage have been practically suppressed; hence power factor obtained is close to one.

Keywords: *Grid-connected, Inverter, Photovoltaic, PI controller, Resonant controller*

1. Introduction

PI controller is the most controller used in regulation loops due to its simplicity and high performances. This controller gives good performances when used for regulating parameters with slow variations. However, for fast variations parameters like currents, this controller is not a good solution; it gives mediocre results due to the presence of following error when the reference is sinusoidal. Moreover control of PV-grid connected inverter introduces a delay between sinusoidal current reference and measured current at the output of the inverter. This leads to a phase difference between the current injected by the inverter and grid voltage when using a simple PI controller. In this paper we will present an alternative to this controller using resonant controller. We will demonstrate that with this solution, phase difference between current and voltage could be suppress; hence, power factor could be considerably improved.

2. Presentation of the System

The studied system is shown in Figure 1. Inverter input is given by a DC/DC converter. The output is connected to the grid via a current filter *RL*. The EMR (Energetic Macroscopic Representation) of DC/DC bloc is represented in Figure 2. The EMR of the system with its control is represented in Figure 3.

In this paper we will not detail the model of this system which is well known (see [1]). However, we must clarify some points about its control.

Control low of each block of the system is deduced by inversion of the EMR of the model of this bloc. First, the MPP (Maximum Power Point) is determined by the MPPT (Maximum Power Point Trucker); optimum voltage of the PV generator (PVG) Vpvref is the reference of the control loop of PVG voltage.

ISSN: 2005-4262 IJGDC

The MPPT used in this study is a "perturb and observe" MPPT based on fuzzy logic [2]. A compensation of the output of PVG voltage loop, by measured current of the PVG, allows obtaining the reference of the control loop of the current traversing *Lpv*:

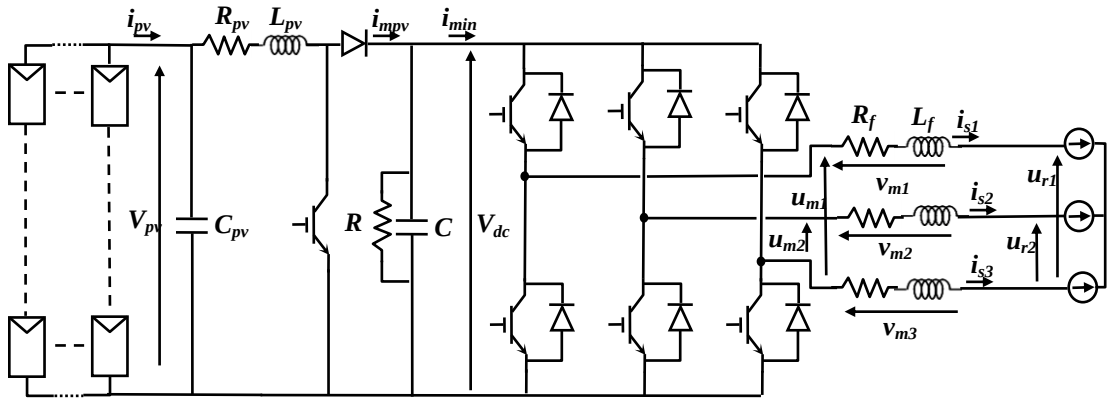

Figure 1. Studied System

$$i_{lref} = PI\,(V_{pvref} - V_{pv}) + i_{pv} \tag{1}$$

Where *PI* is a PI controller.

Controlling induction current i_l and a compensation of V_{pv} by the measured voltage of the GPV allows obtaining the reference of the modulated DC voltage:

$$V_{mref} = PI\,(i_{lref} - i_l) + V_{pv} \tag{2}$$

Finally, a division of the output of this loop by the measured DC voltage leads to the duty cycle *m* which is using to generate the control signal of the DC-DC converter:

$$m_{ref} = \frac{V_{mref}}{V_{dc}} \tag{3}$$

To control the inverter, first, a reference of the DC voltage loop is imposed; a control of DC voltage and a compensation of DC current allow obtaining the reference of the modulated inerter current:

$$i_{mond\_ref} = i_{dc} - PI\,(V_{dc\_ref} - V_{dc}) \tag{4}$$

Using this reference with measured DC voltage, measured two composed voltages and by assuming the conservation of the power in the two sides of the inverter, we calculate the references of the injected currents to the grid by resolving the following system:

$$\begin{pmatrix} P \\ Q \end{pmatrix} = \begin{pmatrix} u_{r1} & u_{r2} \\ \frac{2u_{r2} - u_{r1}}{\sqrt{3}} & \frac{u_{r2} - 2u_{r1}}{\sqrt{3}} \end{pmatrix} \begin{pmatrix} i_{s1} \\ i_{s2} \end{pmatrix} \tag{5}$$

Where reactive power Q is equal to zero and active power P is approximated by:

$$P_{ref} \approx i_{mond\_ref} \cdot V_{dc} \quad (6)$$

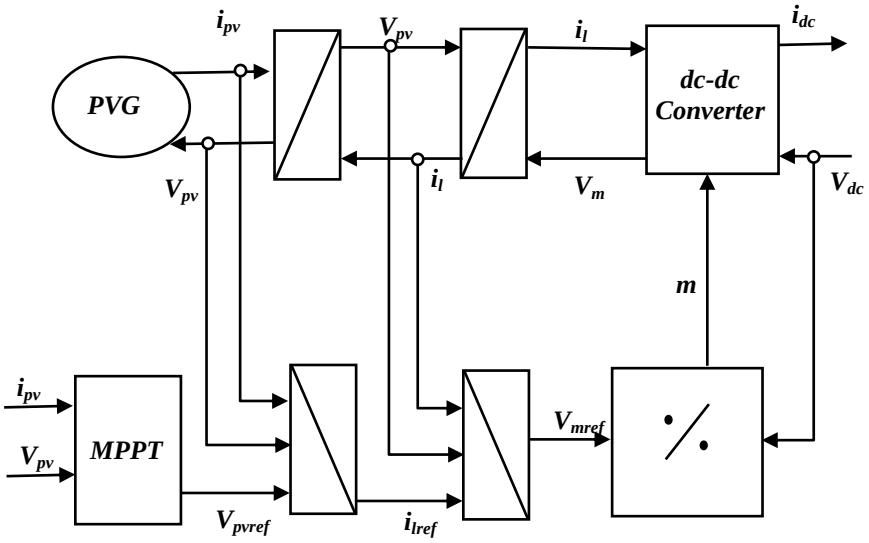

Figure 2. EMR of DC/DC Bloc and its Command

The currents are obtained by two control loops using these two references. After compensation of the composed grid voltages, we obtain references of the modulated composed voltages:

$$u_{m1ref} = REG\ (i_{s1ref} - i_{s1}) + u_{r1} \quad (7)$$

$$u_{m2ref} = REG\ (i_{s2ref} - i_{s2}) + u_{r2} \quad (8)$$

Where *REG* is a PI controller or a resonant controller.

Finally by dividing these references by measured DC voltage we obtain the two ratios m_1 and m_2.

$$< m_1 > = \frac{u_{m1ref}}{V_{dc}} \quad (9)$$

$$< m_2 > = \frac{u_{m2ref}}{V_{dc}} \quad (10)$$

Switches control is then deduced using the method described in [3].

The synchronization of the currents with the grid is ensured by an SVF-PLL. This PLL is described in [4], [5], and [6].

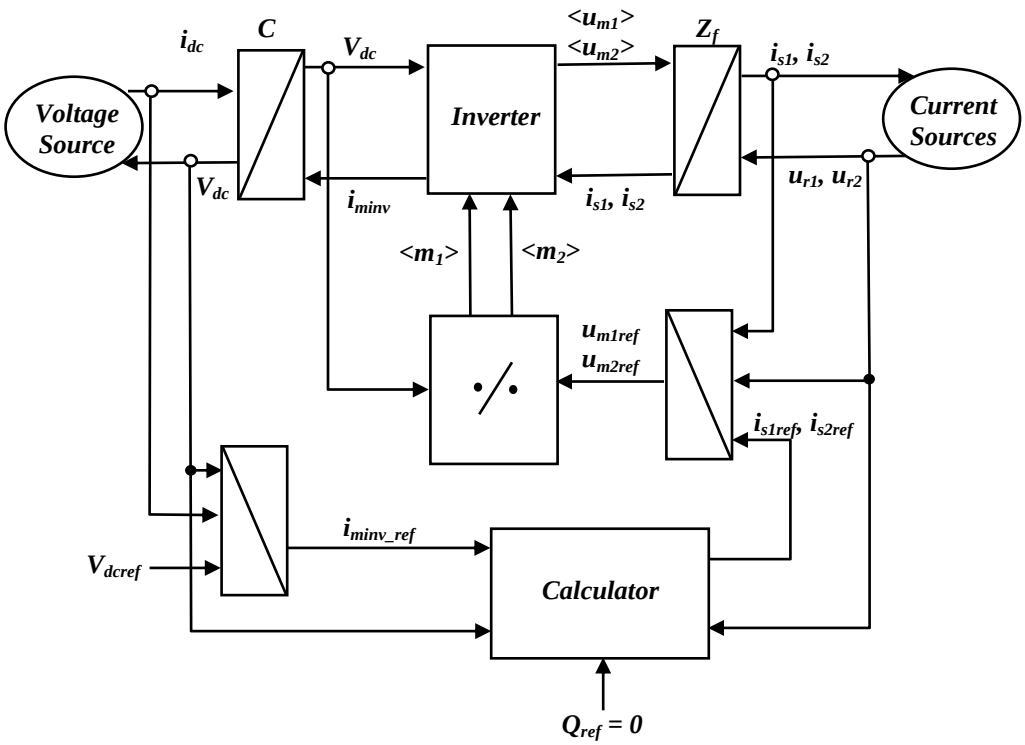

Figure 3. EMR of the System with its Command

3. Control Loops

The first simulation was performed using PI controllers for all the control loops. The parameters of these controllers are deduced by a pole placement. Damping of the system has been taken equal to 1 and time-response equal to 0.01 second.
In the second simulation, the PI controllers of the control loops of currents injected to the grid are substituted by resonant controllers.

The principle of resonant controller is based on the resonance; the transfer function module takes a very big value (infinite in theory) for a privileges frequency, this allows to obtain a difference between the controlled variable and a sinusoidal reference equal to zero[7][8].

The chosen transfer function for this controller is [7][9]:

$$RC(s) = K\frac{(1+\tau_1 s)(1+\tau_2 s)}{\omega_o^2 + s^2} \quad (11)$$

The transfer function of the *RL* filter is given by:

$$T_f = \frac{K_f}{1+\tau_f s} \quad (12)$$

Where:

$$K_f = \frac{1}{R_f} \text{ and } \tau_f = \frac{L_f}{R_f} \quad (13)$$

The model of the inverter is a first order function that takes into account the mean delay τ_{inv} introduced by inverter control [10]:

$$T_{inv} = \frac{1}{1 + \tau_{inv} s} \tag{14}$$

Hence the transfer function of the set inverter-filter is given by:

$$T = \frac{K_f}{(1 + \tau_f s)(1 + \tau_{inv} s)} \tag{15}$$

By taking $\tau_1 = \tau_f$, we obtain the open loop transfer function grouping the inverter, the filter and the resonant controller:

$$T_{SO} = \frac{KK_f(1 + \tau_2)}{(1 + \tau_{inv} s)(\omega_o^2 + s^2)} \tag{16}$$

To determine resonant controller parameters, we used symmetrical optimum method [9]. This method consists in identifying open loop transfer function to the following function:

$$H_{SO} = \frac{\omega^2(2s + \omega)}{s^2(s + 2\omega)}, \quad \omega = \frac{1}{\tau} \tag{17}$$

Where τ is the smallest time-constant of the system.

To the double integration ($1/s^2$) of H_{SO}, we substitute the term $\frac{1}{\omega_o^2 + s^2}$ [9]. Hence H_{SO} became:

$$H_{SO} = \frac{\omega^2(2s + \omega)}{(\omega_o^2 + s^2)(s + 2\omega)} \tag{18}$$

By comparing T_{SO} and H_{SO}, we find:

$$\begin{cases} \dfrac{KK_f}{\tau_{inv}} = \omega^3 \\ \dfrac{\tau_2 KK_f}{\tau_{inv}} = 2\omega^2 \\ 2\omega = \dfrac{1}{\tau_{inv}} \end{cases} \tag{19}$$

Hence:

$$\tau_2 = 4\tau_{inv} \text{ and } K = \frac{1}{8K_f\tau_{inv}^2} \tag{20}$$

Where:

$$\tau_{inv} = \frac{2}{f_c} \tag{21}$$

Where f_c is inverter commutation frequency.

4. Simulation Results

System simulation has been performed in Matlab/SIMULINK environment. Table 1 show parameters used in the Simulations.

DC voltage is taken 600 volts, superior to the amplitude of the grid voltage; this allows the energy to transit from GPV to the grid. Insulation and temperature are fixed to 1000W/m² and 25℃ respectively. Switches forming the inverter are assumed ideal; the effects of encroachment and overlap have been neglected.

Table 1. System Parameters

Parameter	value
C_{pv} : GPV capacitance	5.10^{-3}F
L_{pv} , R_{pv}: GPV inductance	$2.5.10^{-3}$H ,0.01Ω
V_{dc}: DC voltage	600V
C, R : DC capacitance and resistance	3.10^{-3}F, 10^5 Ω
L_f, R_f : Current filter parameters	0.03H, 3Ω
P_{rated} : Panel rated power	110W
N_S : Number of panels in series	3
N_P : Number of panels in parallel	7
f_c : Commutation frequency	5KHz

4.1. PI Controller

Figure 4 shows the three grid currents obtained using PI controllers. Figure 5 shows the current and the voltage of one phase. We can see phase deference between the current and the voltage, the power factor is calculated as following:

$$PF \approx \frac{\cos \varphi_1}{\sqrt{1 + THD^2}} \text{ [11]} \quad (22)$$

Where φ_1 is the phase difference between current and voltage fundamentals.

In this case PF is equal to 0.9743; this means that a reactive power is transmitted to the grid. Current spectrum, normalized in relation to the fundamental, of one phase is shown in Figure 6 and Figure 7. We can see a harmonic pollution around rank 100 even for odd and even harmonics. This is due to the commutation frequency equal to 5 kHz. Third harmonic component magnitude is about 1.4% in this case. It can be seen that low-order even harmonics magnitude is important.

The THD obtained here is equal to 3.90% and DC component is equal to 0. 0.062%.

4.2. Resonant Controller

In this simulation, PI controllers of injected currents control loops have been substituted by resonant controllers.

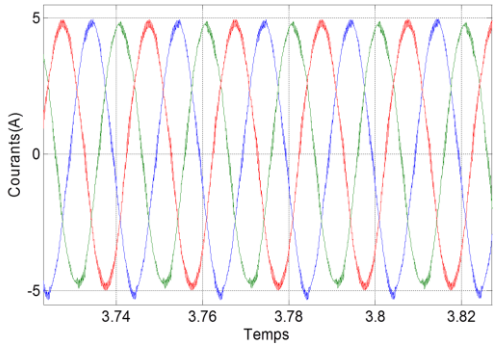

Figure 4. Three Phase Currents

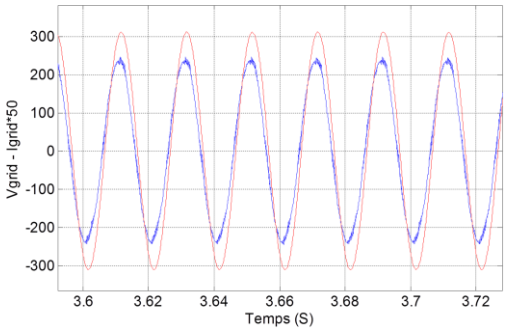

Figure 5. Phase 2 Current and Voltage

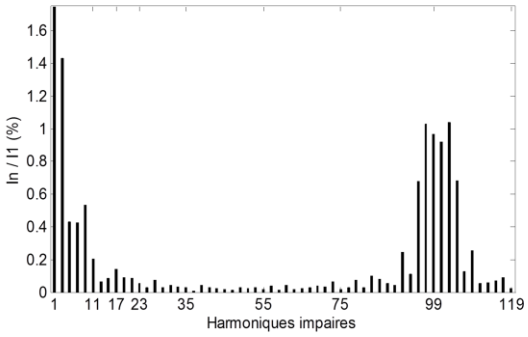

Figure 6. Current odd Harmonics (PI controller)

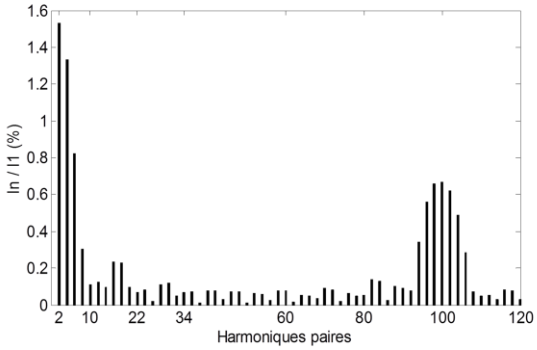

Figure 7. Current even Harmonics (PI Controller)

Figure 8 shows the three grid currents obtained using resonant controllers; their form is better compared to the currents obtained using PI controllers. Current and voltage in Figure 9 are in phase. The power factor in this case is equal to 0.9976 witch is clearly improved in relation to the precedent. The spectrum of phase 2 (Figure 10, Figure 11) shows a harmonic pollution around rank 100 due to the commutation frequency. Third harmonic component magnitude is less than 0.14% in this case which is more than 10 times less than PI controller. It can be seen that low-order even harmonics magnitude in Figure 11 is significantly reduced compared to Figure 7. The THD obtained here is equal to 2.96% and the continue component is equal to 0.19%.

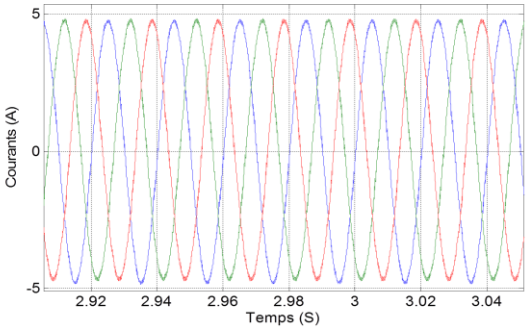

Figure 8. Three Phase Currents

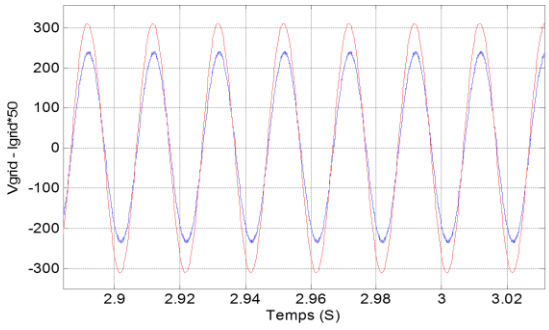

Figure 9. Phase 2 Current and Voltage

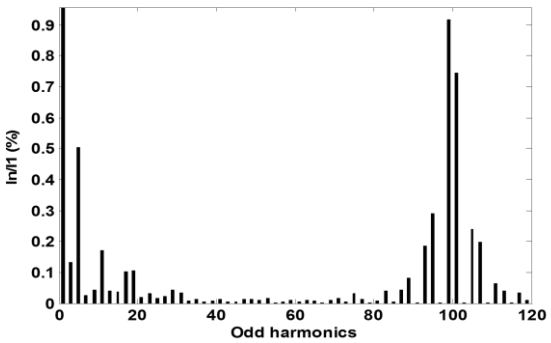

Figure 10. Current odd Harmonics (Resonant Controller)

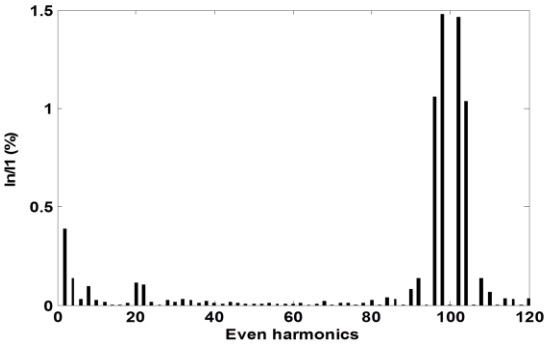

Figure 11. Current even Harmonics (Resonant corrector)

5. Conclusion

This study proves that PI controller is not a good solution for controlling injected currents to the grid because it generates a phase difference between current injected and grid voltage; this means that a reactive power is introduced to the grid. By substituting PI controller by resonant controller, to control injected currents to the grid, a power factor close to zero has been obtained. By using resonant controller, third harmonic component magnitude has been decreased more than 10 times less than PI controller. Moreover low-order even harmonics magnitude has been significantly reduced.

References

[1] N. Hamrouni, M. Jraidi, A. Cherif, "New Control Strategy for 2-Stage Grid-Connected Photovoltaic Power System", Renewable Energy, vol. 33, **(2008)**, pp. 2212-2221.
[2] S. Makhloufi, R. Abdessemed, "Type-2 Fuzzy Logic Optimum PV/Inverter Sizing Ratio for Grid-Connected PV Systems: Application to Selected Algerian Locations", Journal of Electrical Engineering & Technology, vol. 6, no. 6, **(2011)**, pp. 731-741.
[3] A. Bouscayrol, "Formalisme de Représentation et de Commande Appliqués Aux Systèmes Electromécaniques Multimachines Multiconvertisseurs", Habilitation à Diriger des Recherches, H405, **(2003)**.
[4] Y. Pankow, "Etude de l'intégration de la Production Décentralisée Dans un Réseau Basse Tension", Application au Générateur Photovoltaïque, Thèse de Doctorat de l'Ecole Nationale Supérieure d'Arts et Métiers, **(2004)**.
[5] J. Svenson, "Synchronization Methods for Grid Connected Voltage Source Converter, IEE Proc.-Gener. Transm. Distrib., vol 148, no. 3, **(2001)**.
[6] E. F. Mogoş, "Production Décentralisée dans les Réseaux de Distribution", Etude Pluridisciplinaire de la Modélisation pour le Contrôle des Sources, Thèse de Doctorat de l'Ecole Nationale Supérieure d'Arts et Métiers, Centre de Lille, **(2005)**.
[7] F. Vandecasteele, "Alimentation Optimisée d'une Machine Asynchrone Diphasée à Commande Vectorielle", Thèse de Doctorat Université des Sciences et Technologies de Lille, **(1998)**.
[8] Y. Sato, T. Ishizuka, K. Nezu and T Kataoka, "A New Strategy for Voltage-type PWM Rectifiers to Realise Zero Steady-state Control Error in Input Current", IEEE Transactions on Industry Applications, vol. 34, no. 3, **(1998)**, pp. 480-485.
[9] J. Pierquin, "Contribution à la Commande des Système Multimachines Multiconvertisseurs", Thèse de Doctorat Université des Sciences et Technologies de Lille, **(2002)**.
[10] J. P. Louis, B. Multon, Y Bonnassieux, M. Lavabre, "Commande des Machines à Courant Continu à Vitesse Variable", Traité de Génie Electrique D3610-3611, Techniques de l'ingénieur, **(1988)**.
[11] "Guide Détection et Filtrage des Harmoniques", Schneider Electric, **(2008)**.

